

Point Defect Creation by Proton and Carbon Irradiation of α -Ga₂O₃

Alexander Y. Polyakov¹, Vladimir I. Nikolaev^{2,3}, Igor N. Meshkov⁴, Krzysztof Siemek^{4**}, Petr B. Lagov^{1,5}, Eugene B. Yakimov^{1,6}, Alexei I. Pechnikov^{2,3}, Oleg S. Orlov⁴, Alexey A. Sidorin⁴, Sergey I. Stepanov^{2,3}, Ivan V. Shchemerov¹, Anton A. Vasilev¹, Alexey V. Chernykh¹, Anton A. Losev⁷, Alexandr D. Miliachenko⁷, Igor A. Khrisanov⁷, Yu.S. Pavlov⁵, U.A. Kobets⁸ and Stephen J. Pearton^{9*}

¹. National University of Science and Technology MISiS, Moscow, Leninsky pr. 4, Moscow 119049, Russia

². Ioffe Institute, 26 Polytekhnicheskaya Str., St. Petersburg 194021, Russia

³. Perfect Crystals LLC, 28 Politekhnicheskaya str., 194064 St. Petersburg, Russia

⁴. Joint Institute for Nuclear Research, Joliot-Curie 6, Dubna, Moscow Region, 141980, Russian Federation

⁵. Laboratory of Radiation Technologies, A. N. Frumkin Institute of Physical Chemistry and Electrochemistry Russian Academy of Sciences (IPCE RAS), Moscow 119071, Russia

⁶. Institute of Microelectronics Technology and High Purity Materials, Russian Academy of Sciences, 6 Academician Ossipyan str., Chernogolovka, Moscow Region 142432, Russia

⁷. Institute for theoretical and experimental physics NRC “Kurchatov institute”, B.Cheremushkinskaya 25, Moscow, 117218, Russian Federation

⁸. Institute for Physics and Power Engineering, Bondarenko sq. 1, Obninsk, 249033, Russian Federation

⁹. Department of Materials Science and Engineering, University of Florida, Gainesville, FL 32611

**Current address: Institute of Nuclear Physics Polish Academy of Sciences, Krakow, PL-31342, Poland

*Corresponding author: E-mail: spear@mse.ufl.edu

ABSTRACT

This is the author's peer reviewed, accepted manuscript. However, the online version of record will be different from this version once it has been copyedited and typeset.
PLEASE CITE THIS ARTICLE AS DOI: 10.1063/1.50100359

Films of α -Ga₂O₃ grown by Halide Vapor Phase Epitaxy (HVPE) were irradiated with protons at energies of 330 keV, 400 keV and 460 keV with fluences $6 \times 10^{15} \text{ cm}^{-2}$ and with 7 MeV C⁴⁺ ions with fluence of $1.3 \times 10^{13} \text{ cm}^{-2}$ and characterized by a suite of measurements, including Photoinduced Transient Current Spectroscopy (PICTS), Thermally Stimulated Current (TSC), Microcathodoluminescence (MCL), Capacitance-frequency (C-f), photocapacitance and Admittance Spectroscopy (AS) as well as by Positron Annihilation Spectroscopy (PAS). Proton irradiation creates a conducting layer near the peak of the ion distribution and vacancy defects distribution, and introduces deep traps at $E_c - 0.25 \text{ eV}$, $E_c - 0.8 \text{ eV}$, $E_c - 1.4 \text{ eV}$ associated with Ga interstitials, gallium–oxygen divacancies $V_{\text{Ga}}-V_{\text{O}}$, and oxygen vacancies V_{O} . Similar defects were observed in C implanted samples. The PAS results can also be interpreted by assuming the observed changes are due to the introduction of V_{Ga} and $V_{\text{Ga}}-V_{\text{O}}$.

I. INTRODUCTION

The ultra-wide bandgap Ga_2O_3 and related solid solutions are of great interest because of their potential for developing new generation high-power electronic devices and solar-blind photosensitive photodetectors [1-6]. To this point, most effort has been concentrated on the thermodynamically stable monoclinic $\beta\text{-Ga}_2\text{O}_3$ polytype [1-3], but the two metastable polytypes, corundum $\alpha\text{-Ga}_2\text{O}_3$ and rhombohedral $\kappa\text{-Ga}_2\text{O}_3$ have also attracted recent attention. In the case of $\alpha\text{-Ga}_2\text{O}_3$, this is related to a larger bandgap (5.3 eV cf. 4.8 eV in $\beta\text{-Ga}_2\text{O}_3$), higher symmetry, the hope to achieve effective p-type doping [5, 7,8], while $\kappa\text{-Ga}_2\text{O}_3$ has a strong spontaneous electrical polarization opening the way to polarization doping in $\kappa\text{-Ga}_2\text{O}_3$ heterojunctions [5, 9] similar to the case of the AlGaIn/GaN system [10].

One of the attractive features of the Ga_2O_3 system is a high radiation tolerance which makes it suited to harsh radiation environments, such as space applications [11, 12]. For the $\beta\text{-Ga}_2\text{O}_3$ system, experiments on radiation effects have been reported for crystals, films, and devices [5, 11]. The radiation tolerance of $\beta\text{-Ga}_2\text{O}_3$ has been found to be at least on par with AlGaIn/GaN and SiC based devices and much higher than for Si or GaAs [5]. Detailed studies of the changes in electrical, luminescent and recombination properties for proton, neutron, alpha-particles and γ -irradiation have been reported and, in some cases, the identity of the defects has been understood based on comparisons with detailed theoretical modeling [5, 11, 13]. In those studies, the use of Positron Annihilation Spectroscopy (PAS) [14] proven very useful. This technique has been extensively used previously for detecting vacancy-like defects in GaN, AlN, AlGaIn [14-16] has been instrumental in revealing the role of Ga vacancies, V_{Ga} , extended Ga vacancies, V_{Ga}^i (essentially complexes of off-center Ga vacancies and various types of off-center Ga interstitials [13, 17]), and their complexes with hydrogen in compensation of n-type conductivity in proton-irradiated $\beta\text{-Ga}_2\text{O}_3$ [18]. An interesting feature of PAS experiments in $\beta\text{-Ga}_2\text{O}_3$ is the strong anisotropy of the signal due to the anisotropic structure of the predominant radiation defects of V_{Ga}^i [19, 20]. Polymorphism of Ga_2O_3 and the sensitivity of the formation energy of different

polymorphs to strain have been also shown to give rise to unusual polymorphic transitions in heavily irradiated β -Ga₂O₃ that can be converted to κ -Ga₂O₃ [21].

For α -Ga₂O₃, work on identifying the nature of radiation defects is at a preliminary stage. There have been initial studies of radiation damage by monitoring the Rutherford Back Scattering (RBS) in undoped α -Ga₂O₃ subjected to high doses during ion implantation [22]. These studies performed in comparison with GaN and β -Ga₂O₃ suggest a higher radiation tolerance of the α -Ga₂O₃ polymorph.

In this paper, we report the results of proton and carbon irradiation of undoped α -Ga₂O₃ films prepared by Halide Vapor Phase Epitaxy (HVPE) and assessed by electrical and Micro-cathodoluminescence (MCL) measurements and by PAS. A variety of defect complexes are identified.

II. EXPERIMENTAL

II.1. Films growth

Ga₂O₃ films were grown in a custom atmospheric pressure, horizontal quartz HVPE reactor on basal plane sapphire substrates. Gallium chloride (GaCl) and oxygen (O₂) were used as precursors. GaCl was synthesized *in situ* by passing gaseous hydrogen chloride (HCl, 99.999% pure) over metallic gallium (Ga, 99.9999% pure) at 600°C. The GaCl and O₂ were then mixed in the deposition zone of the reactor to produce Ga₂O₃ on the substrate. Argon was used as a carrier gas to keep the total gas flow rate through the reactor at 10 slm. The deposition temperature was 500°C. The VI/III (O₂/GaCl) ratio was 4.2. Under these conditions, the growth rate was 2.4 $\mu\text{m/h}$. X-ray analysis showed that the films were single-phase α -Ga₂O₃. The full width at half maximum (FWHM) of the symmetric (0006) reflection was 13-15 arcminutes (900"), for the asymmetric (10-18) reflection the FWHM was 14-17 arcminutes (1020") (showing that the densities of the screw dislocations were about $4 \times 10^8 \text{ cm}^{-2}$ and of edge dislocations of about $2 \times 10^9 \text{ cm}^{-2}$). The thickness of the films was 4.5 μm and they were not intentionally doped.

II.2. Irradiations

The samples were irradiated with hydrogen and carbon, both of which are important technological impurities in Ga₂O₃ and useful for modeling defect formation in radiation tolerance experiments. Proton irradiation was performed using the "Tandem-3M" machine routinely employed for adjusting parameters of Si power devices [23]. Proton energies of 330 keV, 400 keV, and 460 keV were used. The total proton fluence in all cases was $6 \times 10^{15} \text{ cm}^{-2}$ accumulated at the flux of $6 \times 10^{12} \text{ cm}^{-2}\text{s}^{-1}$.

C⁴⁺ ion irradiation was performed in the I-3 machine with a laser source that serves as an injector for circular accelerator operating in the GeV energy range of accelerated particles [24]. In our experiment the I-3 machine was used independently to irradiate the samples with C⁴⁺ ions of 7 MeV energy per nucleon with a total fluence of $1.3 \times 10^{13} \text{ cm}^{-2}$. The machine was operated in the pulsed regime with frequency of 0.14 Hz and the C⁴⁺ fluence accumulated during each pulse equal to $6.4 \times 10^9 \text{ cm}^{-2}$. Such system is commonly used for trimming the performance of Si diodes in lieu of irradiations with high energy electrons [25, 26].

The ion and related damage profiles (the latter characterized by the density of Ga vacancies) were obtained from the Stopping-and-Range-of-Ions-in-Matter (SRIM) code [27, 28], which calculates the screened Coulombic collision rate between an incoming ion and the atoms in the target material. The results are presented in Fig. S1(a, b) in the Supplementary material.

II.3. Electrical characterization, deep traps, luminescence

For electrical characterization, Ohmic contacts were prepared by e-beam evaporation of Au/Ti (80 nm/20 nm) and Rapid thermal Annealing in N₂ at 350°C for 2 minutes. Circular Ni Schottky diodes 1 mm in diameter and 20 nm thicknesses were made by e-beam evaporation at room temperature through a shadow mask. Electrical characterization involved current-voltage (I-V) measurements of the Schottky diodes in the dark and with monochromatic illumination, current-temperature (I-T), capacitance-frequency (C-f) in the dark and under monochromatic illumination, capacitance-voltage (C-V) measurements in the dark and under monochromatic illumination, Admittance Spectra (AS) [29] (i.e. measurements of temperature dependence of

capacitance and AC conductance G at various frequencies), Thermally Stimulated Current (TSC) [30], Photoinduced Current Transient Spectroscopy (PICTS) [31], and capacitance Deep Level Transient Spectroscopy with optical injection (ODLTS) [29]. For optical excitation, we used a set of high-power (optical power density 250 mW/cm^2) Light-Emitting Diodes (LEDs) with wavelengths ranging from 365-940 nm. For above-bandgap excitation, 259 nm wavelength LEDs with optical power density 1.2 mW/cm^2 were used. These measurements were done in the temperature range 77-500K [30, 32, 33].

Luminescent properties before and after irradiation were measured by Micro-cathodoluminescence (MCL) at room temperature, combined with Secondary Electron (SE) imaging of the surface using a Scanning Electron Microscope JSM 6490 (Jeol, Japan) with MonoCL-3 system.

II.4. PAS measurements

Positron annihilation measurements were done using a monochromatic variable energy positron beam at JINR, Dubna. The beam is based on a ^{22}Na isotope source and frozen neon moderator. After moderation, slow positrons are accelerated using an electric field applied to the sample holder. During the experiment, the positron energy was varied from 0.1 to 20 keV, which determines implantation depth. The mean implantation depth \bar{z} can be calculated using

$$\bar{z} = \frac{A}{\rho} E^n \quad (1)$$

where: A , n are parameters, ρ is the sample density and E is the energy of implanted positrons. In this investigation, the respective values were assumed to be : $n=1.773$, $A=2.36 \mu\text{g}/(\text{cm}^2\text{keV}^{-n})$, and $\rho=6.44 \text{ g/cm}^3$ [4,5]. For each measurement, an energy spectrum of annihilation quanta was recorded and the broadening of the annihilation line analyzed. A HPGe detector ORTEC GEM25P4-70 with an energy resolution (FWHM) of 1.20 keV at 511 keV was used. This method is known as Doppler broadening of annihilation line spectroscopy (DBS) [34].

It is a common practice to characterize the measured spectra by the S and W parameters that stand respectively for the number of counts below the central and wing part of the

annihilation line, divided by the total number of counts below this line. [14]. The changes of these parameters give us the information about the momentum of electron in the annihilation site. The S parameter corresponds to annihilation with low momentum electrons (i.e. valence electrons) and W parameter characterizes annihilation with high momentum electrons (core electrons). When positron is localized in a void defect, such as a vacancy, the probability of annihilation with valence electrons increases and causes the enhancement of the S parameter and a decrease of the W parameter. Filling of the vacancy with hydrogen will place the S parameter value between the one observed in the sample with no defects and the S-parameter for empty vacancy. When varying the positron beam energy one can compare the contributions of the surface and interior regions of the sample. The lower positron energy increases the number of positrons annihilated at surface defects. Detailed information about concentration of defects in the near surface zone can be obtained using positron diffusion model, which allows to analyze the rate of decrease of S parameter (or increase of W parameter). In the current work fitting to experimental data was done using e⁺DSc-1 program [35]. In the program, it was assumed that all defects below the surface are uniformly distributed. Three parameters that were fitted were S_{Surface} (or W_{surface}) standing for the contribution of surface defects, S_{interior} (or W_{interior}) for the sample interior, and positron diffusion length L₊. The positron diffusion length is linked with defect concentration and it is shortened when new defects appear. Generally, the defect concentration C_v can be calculated using the equation [36]:

$$C_v = \frac{1}{\mu\tau_{bulk}} \left(\left(\frac{L_{bulk}}{L_+} \right)^2 - 1 \right) \quad (2)$$

where: μ is the trapping coefficient (for a given type of defect), τ_{bulk} is the positron lifetime in the bulk and L_{bulk} is the positron diffusion length. However, due to the lack of information on the type of defect and its rate of trapping, such estimation is not possible. A shorter diffusion length may also be interpreted as the presence of a positive potential at the surface that would repel

positrons towards the bulk. Such interpretation was ruled out based on the works of Lovejoy et al [37] and Swain et al [38].

III.RESULTS AND DISCUSSION

III.1. Electrical characterization, deep traps, MCL spectra

The undoped α -Ga₂O₃ samples were highly resistive at room temperature in the dark, but showed a photocurrent and a low open circuit voltage under illumination (see Figure. 1(a)). The temperature dependence of the dark current had an activation energy ~ 100 meV (Figure 1(b)). Given the high dark resistance this slight temperature dependence suggests the prevalence of the hopping conductivity via deep states. The spectral dependence of photocurrent showed a minor onset around the photon energy of 2 eV and a strong increase for photon energies above 3.1 eV (see Fig. S2 in the Supplementary Material).

The sample showed a TSC signal after cooling down at -20V in the dark and illumination at 100K with 4.8 eV photons for 15 minutes, with subsequent heating up at -20V with temperature ramp rate of 1.5 K/s. The differential spectra displayed two peaks and respective activation energies estimated as $E_a = 23 k_B T(\text{peak})$ [32, 33] were ~ 0.5 - 0.6 eV (k_B here is the Boltzmann constant and $T(\text{peak})$ is the temperature of the peak in TSC spectrum) (Figure 2) .

PICTS spectra, i.e. the temperature dependence of the differential transient photocurrent signal $\Delta I_{\text{ph}}(t)$ measured at time windows t_1 and t_2 ($t_2 \gg t_1$, in actual experiment $t_2 = 10t_1$), $\Delta I = I_{\text{ph}}(t_1) - I_{\text{ph}}(t_2)$ showed two peaks whose position shifted to higher temperature and was determined by the relation $1/t_1 = e_n(T_M)$, where e_n is the electron emission rate from the center responsible for the peak and T_M is the peak temperature obtained for the chosen t_1 value [31-33]. Such spectrum measured at -20V and illumination with the 4.8 eV LED is shown in Figure 3 and displays two electron traps with activation energies 0.5 eV and 0.6 eV. The capacitance of the reference samples was too low to be measured.

In SEM measurements, the surface of the sample was reasonably smooth, but occasionally one observed small approximately round holes with smooth bottom and inclined sidewalls with

the outer diameter $\sim 100\ \mu\text{m}$, the inner diameter $\sim 50\ \mu\text{m}$ decorated by small hillocks (Fig. S3(a) of the Supplementary Material). The MCL spectra of the smooth surface displayed the common $\alpha\text{-Ga}_2\text{O}_3$ broad band extending from 4 eV to 2 eV and peaked at $\sim 3\ \text{eV}$ [6, 39]. In the area of the hillocks surrounding the holes, one observed an increase in the overall MCL intensity and the shift of the effective peak position to higher energy, so that, when observed in the high energy MCL the hillocks created a bright halo (Fig. S3 (b) of the Supplementary Material). The spectra measured on the flat portion of the sample and around the hillocks are shown in Fig.S4.

The traps in these samples in TSC and PICTS are similar to those detected in conducting Sn doped $\alpha\text{-Ga}_2\text{O}_3$ films earlier [39]. The optical threshold near 3.1 eV observed in the current-voltage spectra of the undoped films is also similar to that observed in photocapacitance spectra of n-type films [39]. Recent theoretical modeling results for $\alpha\text{-Ga}_2\text{O}_3$ suggest that these states could be due to Ga vacancies V_{Ga} acceptors [40].

For the proton irradiated samples, the irradiation increased the dark current, with an activation energy for temperature dependence $>300\text{K}$ of 0.25 eV, which should be close to the position of the proton-induced trap pinning the Fermi level. At higher temperatures, another level at 0.55 eV was observed (Figure 1(b)). The sample showed a much higher photosensitivity than before irradiation with protons, with optical thresholds near 2.3 eV and 2.8 eV. These give the optical ionization energies of the traps introduced by 330 keV protons. The first transition energy is close to the transition level of the oxygen vacancy donor V_{O} predicted by theory [40]. The formation energies of native defects complexes with hydrogen in $\alpha\text{-Ga}_2\text{O}_3$ have not been reported, but judging by the experience with $\beta\text{-Ga}_2\text{O}_3$ [13], the second optical threshold near 2.8 eV could be due to a complex of V_{Ga} with hydrogen. In TSC spectra one observes a marked overall increase of the signal, with the peaks at 0.5-0.6 eV becoming more prominent and the emergence of an additional strong peak corresponding to the level near 0.8 eV from the conduction band edge.

In PICTS spectra one observes an increased amplitude of the 0.5-0.6 eV peaks, a prominent shoulder corresponding to the level with energy close to 0.8 eV from the conduction band edge and a strong peak corresponding to a defect with level near 1.4 eV from either the conduction band or valence band (in PICTS it is difficult to discriminate between centers from the upper and lower half of the bandgap [31-33]). The centers near $E_c-0.8$ eV can be tentatively associated with the upper charge transfer level of the oxygen interstitial acceptors O_{i2} , while the energy of 1.4 eV is close to the predicted charge transfer upper acceptor level of divacancy $V_{Ga}-V_O$ [40]. The sample irradiated with protons showed measurable capacitance in the dark at room temperature (Fig. 6(a)). The capacitance shows two steps with roll-off frequencies close to 1 kHz and 20 kHz, with a strong photocapitance with threshold energies near 1.5 eV, 2 eV, 2.8 eV, and 3.1 eV (Fig. 6(b)). The latter optical threshold could be associated with V_{Ga} [40]. The capacitance value for the low-frequency capacitance step approximately corresponds to the depth at which the peak in the hydrogen ion and vacancy distributions is expected from the SRIM modeling (Figure S1(a)). This suggests the conductivity proceeds via the layer with the high density of hydrogen ions H^+ and radiation defects, while the access resistance is determined by the layer adjacent to the surface in which conductivity is determined by radiation defects, possibly complexed with hydrogen. Admittance spectra (Figure S5 (a, b)) give activation energy of 0.25 eV. These have been previously detected in Sn doped and unintentionally doped α - Ga_2O_3 films [39] and associated with the dominant defect donors in α - Ga_2O_3 , namely Ga interstitials, Ga_i [40].

In MCL measurements performed on the portion of the sample without prominent surface defects, the spectrum was similar to the spectrum before irradiation, but with a lower intensity. However, after irradiation there appeared a lot of defects looking like small hillocks. For these regions the spectrum was dominated by a narrow band peaked near 3.23 eV and showing a high intensity (Figure S4). Figures S6(a, b) of the Supplementary Material illustrate the relation between the presence of defects and the intensity of the 3.23 eV line. The origin of defects causing the surface features and of the 3.23 eV line in MCL is not yet understood.

For samples irradiated with 7 MeV energy C^{4+} ions, the resistivity after irradiation became lower than before irradiation. The temperature dependence of the current at 20V had activation energy of conductivity of 1.1 eV for $T > 300\text{K}$ (Figure 1 (b)). In TSC, the signal was very weak and showed the peaks corresponding to centers at $E_c - 0.6$ eV and $E_c - 0.8$ eV (Figure 2). In PICTS peaks corresponding to centers with energy of 0.8 eV and 1.4 eV were detected (Figure 3). The origin of these traps is the same as in the H-irradiated sample. In MCL measurements the signal for the flat portions of the sample showed the same wide 2-4 eV band peaked near 3 eV as before irradiation, but the MCL intensity was much weaker than before irradiation. Hillock defects similar to those observed for the 330 keV proton irradiated samples were observed at much lower density. The MCL spectra on these defects were similar to the proton irradiated samples, but the intensity was much lower (Figure S4). The results suggest a high density of deep traps decreasing the conductivity, photosensitivity and photoluminescence intensity. Table I summarizes the activation energies of defects observed after irradiation and their proposed attributions based on theoretical modeling.

III.2. PAS results

The results of variable energy beam measurements of the S and W parameters are shown in Figure 5(a, b). From Figure 5(a), the S parameter of all samples substantially decreases when increasing the positron energy (i.e. probed depth of the sample), while proton irradiation enhances this increase, the more so, the higher the proton energy. Carbon irradiation did not strongly alter the results compared to the reference (unirradiated) sample. The situation with the W parameter is at low positron energies mirror-like in respect to the S parameter data, which is expected [14]. However, for high positron energies the reference and proton implanted samples exhibit the same trends for S parameter data, suggesting defects at the surface and in the bulk behave differently. The situation is graphically illustrated by Figure 6 in which the S parameters versus W parameters are plotted as a function of the positron energy. Normally, if one is dealing with only one type of defects, such a plot should show that all points are lying on a line with the

same slope [14]. There is the surface region shallower than ~ 5 nm where the surface S_{surface} and W_{surface} values are related as shown in Figure 7. In this region the S_{surface} (and the density of vacancy-like defects) is the lowest for the reference sample, slightly higher for the C implanted sample, and increases for proton irradiated samples with increasing proton energy. Deeper inside the samples, the slope of the S versus W plot is quite high, but at depths exceeding ~ 10 nm becomes lower and strongly levels off for depths exceeding ~ 200 nm. This behavior is partly due to the positron diffusion to the surface and annihilation at surface defects. Figure 8 presents the positron diffusion lengths L_+ as estimated for the studied samples from the proton diffusion model described in Ref. [35]. The diffusion length is very short, only 22 nm even for the reference sample which can be compared to the value of 90 nm in good quality $\beta\text{-Ga}_2\text{O}_3$ [38]. Proton irradiation further decreased the diffusion length to below 18 nm, while C irradiation had little effect on the positron diffusion length (Figure 8).

If one compares the results with those reported for $\beta\text{-Ga}_2\text{O}_3$ samples one observes significant differences. In $\beta\text{-Ga}_2\text{O}_3$, the dominant PAS feature is due to the split V_{Ga}^i vacancies responsible for a prominent anisotropy of the PAS signal, which is related to the symmetry of the split vacancies V_{Ga}^i that are essentially complexes of off-center vacancies and off-center Ga interstitials that have a well-defined orientation along a certain crystallographic direction in $\beta\text{-Ga}_2\text{O}_3$ [19, 20]. Proton irradiation introduces new defects with features compatible with isolated Ga vacancies and their complexes with hydrogen, as evidenced by Local Vibrational Mode (LVM) spectra measurements, as well as passivation with hydrogen of the split vacancies PAS feature and shortening of the positron lifetime. The results also indirectly suggest that $V_{\text{Ga}}\text{-}V_{\text{O}}$ divacancies could be a part of the radiation defects ensemble and could be responsible for the formation of prominent radiation defects, the $E2^*$ centers [13, 18].

Theoretical studies for $\alpha\text{-Ga}_2\text{O}_3$ [40] do not predict the formation of defects similar to the split Ga vacancies in $\beta\text{-Ga}_2\text{O}_3$, which is confirmed by the absence of anisotropy of the Doppler broadening of the main PAS feature for the $\alpha\text{-Ga}_2\text{O}_3$ samples. Judging by comparison with the

results of electrical measurements and deep trap spectra, the likely candidates for the role of defects seen in PAS experiments are the Ga vacancies, their complexes with hydrogen, and $V_{\text{Ga}}-V_{\text{O}}$ divacancies (oxygen vacancies that are predicted to be deep donors in $\alpha\text{-Ga}_2\text{O}_3$ as in $\beta\text{-Ga}_2\text{O}_3$ and have been shown not to be efficient positron recombination sites in $\beta\text{-Ga}_2\text{O}_3$ [14, 18-20]). The introduction of V_{Ga} -related defects is likely also responsible for the shortening of the positron diffusion length in irradiated samples, which would be in line with the recently published PAS results for $\beta\text{-Ga}_2\text{O}_3$ crystals subjected to annealing in O_2 atmosphere that resulted in the reduction of the positron diffusion length from 90 nm to 6-10 nm [38].

CONCLUSIONS

The undoped HPVE films had a high resistivity and low activation energy of conductivity of ~ 100 meV, suggesting predominant hopping conductivity via a band of deep states. TSC and PICTS spectra show the presence of $E_c-(0.5-0.6)$ eV traps similar to the traps observed in conducting Sn doped $\alpha\text{-Ga}_2\text{O}_3$ samples [39]. Photocurrent spectra indicate presence of deep acceptors with optical ionization energy 3.1 eV associated with V_{Ga} acceptors. MCL spectra were dominated by the usual broad band 2 eV-4 eV peaked near 3 eV.

Irradiation with 330-460 keV protons increased the dark current and formed a conducting channel about 2 μm below the surface, close to the location of the peak in implanted H concentration and implantation-induced vacancies concentration. Admittance spectra indicated the access resistance of the irradiated samples determined by radiation defects and showing activation energy of conductivity ~ 250 meV. The temperature dependence of resistivity shows the same activation energy, with the activation energy at temperatures above 400K was due to deeper traps near $E_c-0.55$ eV. PICTS spectra of these H irradiated samples were determined by traps with levels near $E_c-0.5$ eV, $E_c-0.6$ eV, $E_c-0.8$ eV, $E_c-1.4$ eV. The latter two are ascribed to the $V_{\text{Ga}}-V_{\text{O}}$ divacancy states and the V_{O} states, respectively. The photosensitivity and photocapacitance of these samples was high and was determined by the traps with optical ionization thresholds near to 1.4, 2, 2.8, 3.1 eV. H irradiation also create regions with a high

density of small hillock defects of unexplained origin, characterized by a high intensity of a narrow defect band peaked at 3.2 eV.

Irradiation of α -Ga₂O₃ with 7 MeV C⁴⁺ ions was characterized by a low conductivity, with activation energy of 1.1 eV, close to the main peak at E_c-1.4 eV in PICTS spectra attributed to the V_O donor states and possibly also determining the temperature dependence of conductivity. Another prominent peak in PICTS spectra was due to the traps near E_c-0.8 eV ascribed to divacancy states. In PAS spectra, we observed short diffusion length of positrons of 22 nm in reference samples. This diffusion length decreased after proton irradiation but was not strongly affected by C irradiation. The identity of defects giving rise to the PAS signal in the undoped samples needs further studies including modeling, but the data looks compatible with the defects being due to Ga vacancies or V_{Ga}-V_O divacancies.

Supplementary Material

The supplementary material contains additional characterization of the samples, including simulated ion and vacancy distributions, photocurrent for the reference and irradiated samples, some optical and secondary electron images of the samples and capacitance-temperature and micro cathodoluminescent data.

Conflicts of Interest

The authors have no conflicts to declare.

Date Availability

The data that supports the findings of this study are available within the article and its supplementary material.

ACKNOWLEDGMENTS

The work at NUST MISiS was supported in part by the grant from the Ministry of Science and Higher Education of the Russian Federation in the framework of Increase Competitiveness Program of NUST «MISiS» (K2-2022-006). The work at IMT RAS was supported by State Task No 075-00706-22-00. The work at UF was funded by the Defense Threat Reduction Agency

This is the author's peer reviewed, accepted manuscript. However, the online version of record will be different from this version once it has been copyedited and typeset.
PLEASE CITE THIS ARTICLE AS DOI: 10.1063/5.0100359

(DTRA) as part of the Interaction of Ionizing Radiation with Matter University Research Alliance (IIRM-URA) under contract number HDTRA1-20-2-0002. The work at UF was also supported by NSF DMR 1856662 (James Edgar).

REFERENCES

- [1] S. J. Pearton, Jiancheng Yang, Patrick H. Cary IV, F. Ren, Jihyun Kim, Marko J. Tadjer, and Michael A. Mastro, *Appl. Phys. Rev.* 5, 011301 (2018)
- [2] S. J. Pearton, Fan Ren, Marko Tadjer, and Jihyun Kim, *J. Appl. Phys.* 124, 220901 (2018)
- [3] Gallium Oxide: Materials Properties, Crystal Growth, and Devices, ed. Masataka Higashiwaki and Shizuo Fujita (Springer Series in Materials Science ISBN 978-3-030-37152-4 ISBN 978-3-030-37153-1, 2020)
- [4] J. Xu, W. Zheng and F. Huang, *J. Mater. Chem. C*, 7, 8753 (2019).
- [5] Elaheh Ahmadi, and Yuichi Oshima, *J. Appl. Phys.* 126, 160901 (2019).
- [6] A. Y. Polyakov, Vladimir I. Nikolaev, Eugene B. Yakimov, Fan Ren, Stephen J. Pearton, and Jihyun Kim, *J. Vac. Sci. Technol. A* 40, 020804 (2022),
- [7] Kentaro Kaneko, Shizuo Fujita, and Toshimi Hitora, *Japan J. Appl Phys* 57, 02CB18 (2018)
- [8] K. Kaneko, Y. Masuda, Shin-ichi Kan, I. Takahashi, Y. Kato, T. Shinohe, S. Fujita, *Appl. Phys. Lett.* 118, 102104 (2021).
- [9] M. B. Maccioni, and V. Fiorentini, *Appl. Phys. Express* 9, 041102 (2016).
- [10] Matteo Meneghini, Carlo De Santi, Idriss Abid, Matteo Buffolo, Marcello Cioni, Riyaz Abdul Khadar, Luca Nela, Nicolò Zagni, Alessandro Chini, Farid Medjdoub, Gaudenzio Meneghesso, Giovanni Verzellesi, Enrico Zanoni, and Elison Matioli, *J. Appl. Phys.* 130, 181101 (2021).
- [11] Jihyun Kim, Stephen J. Pearton, Chaker Fares, Jiancheng Yang, Fan Ren, Suhyun Kima and Alexander Y. Polyakov, *J. Mater. Chem. C* 7, 10 (2019)
- [12] S.J. Pearton, A. Aitkaliyeva, M. Xian, F. Ren, A. Khachatryan, A. Ildefonso, Z. Islam, Md Abu Jafar Rasel, A. Haque, A.Y. Polyakov and J. Kim, *ECS J. Sol. State Sci. Technol.* 10, 055008 (2021).
- [13] M. E. Ingebrigtsen, A. Y. Kuznetsov, B. G. Svensson, G. Alfieri, A. Mihaila, U. Badstubner, A. Perron, L. Vines, and J. B. Varley, *APL Mater.* 7, 022510 (2019)

- [14] Filip Tuomisto and Ilja Makkonen, *Rev. Mod. Phys* 85, 1583 (2013).
- [15] A. Uedono, S. Ishibashi, S. Keller, C. Moe, P. Cantu, T. M. Katona, D. S. Kamber, Y. Wu, E. Letts, S. A. Newman, S. Nakamura, J. S. Speck, U. K. Mishra, S. P. DenBaars, T. Onuma, and S. F. Chichibu, *J. Appl. Phys.* 105, 054501(2009)
- [16] S. F. Chichibu, A. Uedono, K. Kojima, H. Ikeda, K. Fujito, S. Takashima, M. Edo, K. Ueno, and S. Ishibashi, *J. Appl. Phys* 123, 161413 (2018)
- [17] Peter Deak, Quoc Duy Ho, Florian Seemann, Balint Aradi, Michael Lorke, and Thomas Frauenheim, *Phys. Rev. B* 95, 075208 (2017)
- [18] A. Karjalainen, P. M. Weiser, I. Makkonen, V. M. Reinertsen, L. Vines and F. Tuomisto, *J. Appl. Phys.* 129, 165702 (2021).
- [19] A. Karjalainen, I. Makkonen, J. Etula, K. Goto, H. Murakami, Y. Kumagai, and F. Tuomisto, *Appl. Phys. Lett.* 118, 072104 (2021).
- [20] Antti Karjalainen, Vera Prozheeva, Kristoffer Simula, Ilja Makkonen, Vincent Callewaert, Joel B. Varley and Filip Tuomisto, *Phys Rev B* 102, 195207 (2020)
- [21] Alexander Azarov, Calliope Bazioti, Vishnukanthan Venkatachalapathy, Ponniah Vajeeston, Edouard Monakhov, and Andrej Kuznetsov, *Phys. Rev. Lett.* 128, 015704 (2022)
- [22] A.I. Titov, K.V. Karabeshkin, A.I. Struchkov, V.I. Nikolaev, A. Azarov, D.S. Gogova, P.A. Karaseov, *Vacuum* 200, 111005 (2022),
- [23] P.B. Lago, A.S. Dreni and M.A. Zinoviev, *J. Phys: Conference Series*, 830, 012152 (2017).
- [24] T V Kulevoy, A A Losev, P N Alekseev, Yu A Satov, A V Shumshurov, P B Lagov, M E Letovaltseva, S A Zinoviev, Laser ion source for semiconductor applications, ICIS2021 Conference Paper IOP (in press)
- [25] Y.S. Pavlov and P.B. Lagov (2015) Proceedings of the European Conference on Radiation and its Effects on Components and Systems, RADECS, 2015-December, art. no. 7365629. DOI: 10.1109/RADECS.2015.7365629

- [26] Y.S. Pavlov, A.M. Surma, P.B. Lagov, Y. L. Fomenko and E.M. Geifman, J. Phys.: Conference Series, 747, 012085 (2016).
- [27] See the tutorial and software download site at <http://www.srim.org/>
- [28] J. F. Ziegler, J. P. Biersack, U. Littmark, "The Stopping and Range of Ions in Solids, (Pergamon Press, New York (1984).
- [29] Capacitance spectroscopy of semiconductors, ed. Jian V. Li and Giorgio Ferrari (Pan Stanford Publishing Pte Ltd, Singapore, 2018) 437 pp
- [30] A. Y. Polyakov, N. B. Smirnov, I. V. Shchemerov, E. B Yakimov, S. J. Pearton, F. Ren, A. V. Chernykh, D. Gogova and A. I. Kochkova, ECS J. Sol. State Sci Technol, 8, Q3019 (2019)
- [31] M. Tapiero, N. Benjelloun, J.P. Zielinger, S. El Hamd, and C. Noguet, J. Appl. Phys. 54, 4006 (1988).
- [32] E. B. Yakimov, A. Y. Polyakov, N. B. Smirnov, I. V. Shchemerov, P. S. Vergeles, E. E. Yakimov, A. V. Chernykh, M. Xian, F. Ren and S. J. Pearton, J. Phys. D: Appl. Phys. 53, 495108 (2020).
- [33] A. Y. Polyakov, N. B. Smirnov, I. V. Shchemerov, S. J. Pearton, Fan Ren, A. V. Chernykh, and A. I. Kochkova, Appl. Phys. Lett. 113, 142102 (2018)
- [34] M. Eseev, P. Horodek, V. Khilinov, A. Kobets, V. Kobets, I. Meshkov, O. Orlov, K. Siemek and A. Sidorin, Acta Physica Polonica A. 136. 314 (2019).
- [35] Jerzy Dryzek, Analysis of positron profiling data using e⁺DSc computer code, Computer Phys Commun, 264, 107937(2021).
- [36] R. Krause-Rehberg, V. Bondarenko, E. Thiele, R. Klemm and N. Schell, Nuclear Inst. and Meth. Physics Res. B, 240, 719 (2005)
- [37] T. C. Lovejoy, R. Chen, X. Zheng, E. G. Villora, K. Shimamura, H. Yoshikawa, Y. Yamashita, S. Ueda, K. Kobayashi, S. T. Dunham, F. S. Ohuchi, and M. A. Olmstead, Appl. Phys. Lett. 100, 181602 (2012).

This is the author's peer reviewed, accepted manuscript. However, the online version of record will be different from this version once it has been copyedited and typeset.
PLEASE CITE THIS ARTICLE AS DOI: [10.1063/5.0100359](https://doi.org/10.1063/5.0100359)

- [38] Santosh K. Swain, Marc H. Weber, Jani Jesenovec, Muad Saleh, Kelvin G. Lynn, and John S. McCloy, *Phys. Rev. Appl.* 15 (2021) 054010
- [39] A. Y. Polyakov, V. I. Nikolaev, S. I. Stepanov, A. I. Pechnikov, E. B. Yakimov, N. B. Smirnov, I. V. Shchemerov, A. A. Vasilev, A. I. Kochkova, A.V. Chernykh, and S. J. Pearton, *ECS J. Sol. State Sci. Tech.*, 9, 045003, (2020)
- [40] Takuma Kobayashi, Tomoya Gake, Yu Kumagai , Fumiyasu Oba and Yu-ichiro Matsushita, *Appl. Phys Express* 12, 091001 (2019).

This is the author's peer reviewed, accepted manuscript. However, the online version of record will be different from this version once it has been copyedited and typeset.
PLEASE CITE THIS ARTICLE AS DOI: 10.1063/1.50100359

Table I. Defects detected before and after H or C implantation

| Sample | Defects detected | Possible origin |
|-----------|-------------------|--|
| reference | E_c -0.5-0.6 eV | E_c -0.6 eV A traps in Sn doped α -Ga ₂ O ₃ films [39] |
| | E_c -3.1 eV | V_{Ga}^{3-} [40] |
| H 330 keV | E_c -0.25 eV | E_c -0.25 eV D traps in Sn doped α -Ga ₂ O ₃ films [39], possibly Ga _i donors [40] |
| | E_c -0.55 eV | E_c -0.6 eV A traps in Sn doped α -Ga ₂ O ₃ films [39] |
| | E_c -0.8 eV | E_c -0.8 eV C traps in Sn doped α -Ga ₂ O ₃ films [39], possibly $(V_{Ga}-V_O)^{2-}$ [40] |
| | E_c -1.4 eV | V_O [40] |
| | E_c -2.8 eV | V_{Ga-2H} (?) |
| C 7 MeV | E_c -3.1 eV | V_{Ga}^{3-} [40] |
| | E_c -0.8 eV | $(V_{Ga}-V_O)^{2-}$ [40] |
| | E_c -1.1 eV | V_O (?) |
| | E_c -1.4 eV | V_O [40] |

FIGURE CAPTIONS

Figure 1 (color online) (a) Room temperature I-V characteristics of Ni Schottky diode on the reference sample before irradiation, measured in the dark (black line), with 385 nm illumination (blue line), 365 nm illumination (violet line), and with 259 nm LED illumination (red line); (b) temperature dependence of dark current at 20 V for the reference sample (black line), sample irradiated with 330 keV protons (red line), and sample irradiated with C (olive line)

Figure 2. (Color online) TSC spectra of the reference sample, the sample irradiated with 330 keV protons, and the C irradiated sample.

Figure 3. (Color online) PICTS spectra measured with 259 nm LED excitation (pulse length 5 s) at -20 V, with time windows 350 ms/ 3500 ms for the three samples.

Figure 4. (Color online) (a) Capacitance versus frequency dependence (left axis) and AC conductance normalized by angular frequency, G/ω , measured for the sample irradiated with 330 keV protons in the dark and with monochromatic light of LEDs with peak wavelength from 940 nm to 365 nm; (b) the photocapacitance ΔC_{ph} spectrum

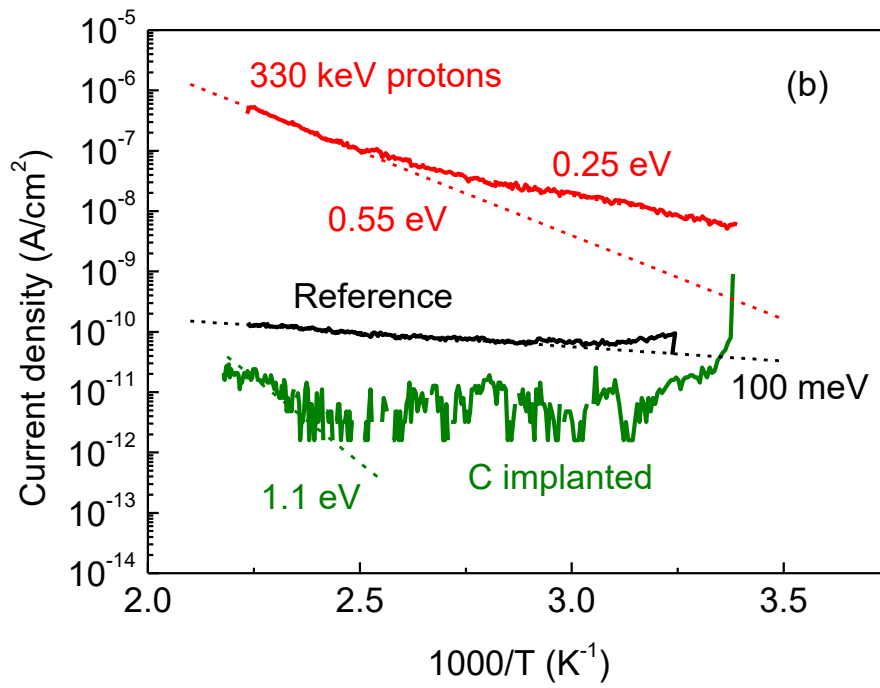
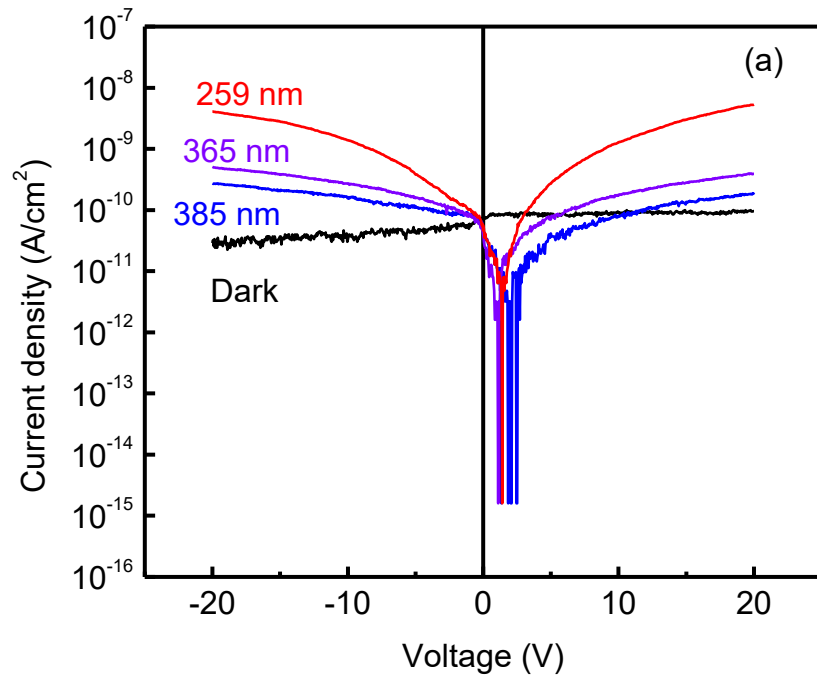
Fig. 5 (Color online) (a) The S parameter dependence on the implanted positron energy. The upper axis corresponds to the mean calculated positron penetration depth; (b) the same for the W parameter. The black lines are the results of fitting

Fig. 6 (Color online). The S-W plot for data in Figure 5. Two slopes marked with arrows indicate the presence of different kinds of defects.

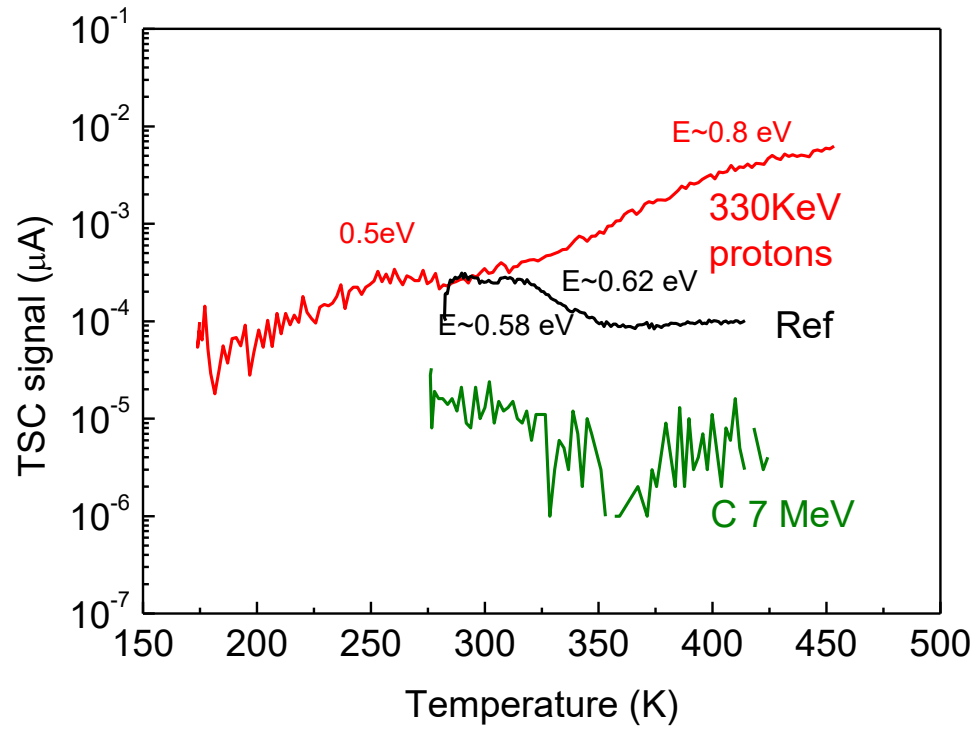
Fig. 7 (Color online). The S-W plots for surface parameters for fitted curves in Figure 5

Fig. 8. Positron diffusion length L_+ obtained using the positron diffusion model.

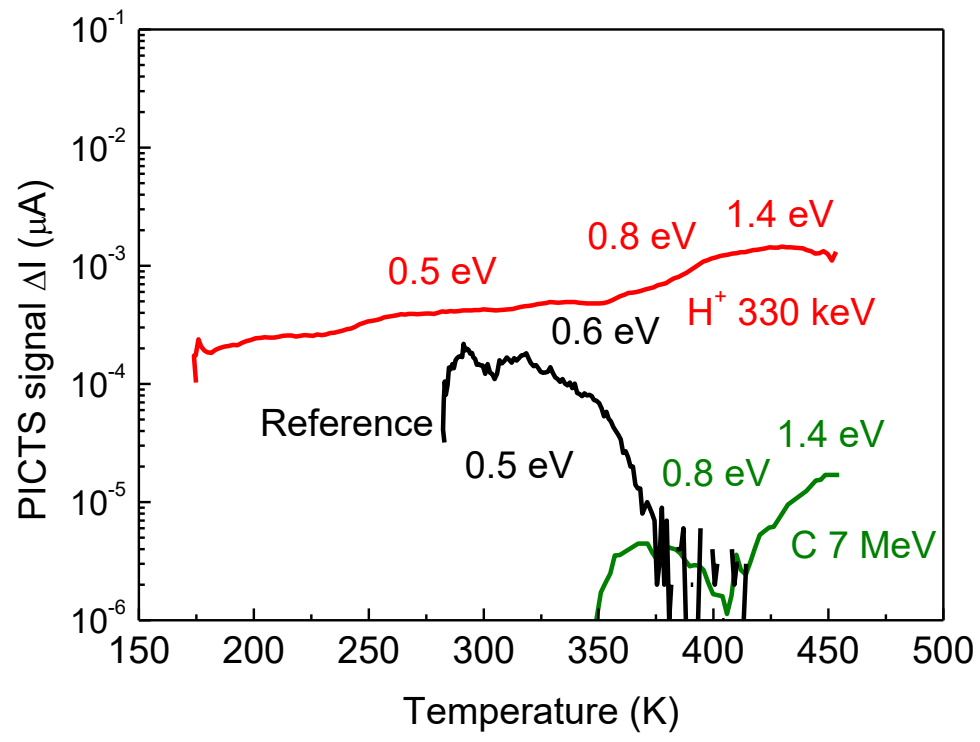
This is the author's peer reviewed, accepted manuscript. However, the online version of record will be different from this version once it has been copyedited and typeset.
PLEASE CITE THIS ARTICLE AS DOI: 10.1063/5.0100359



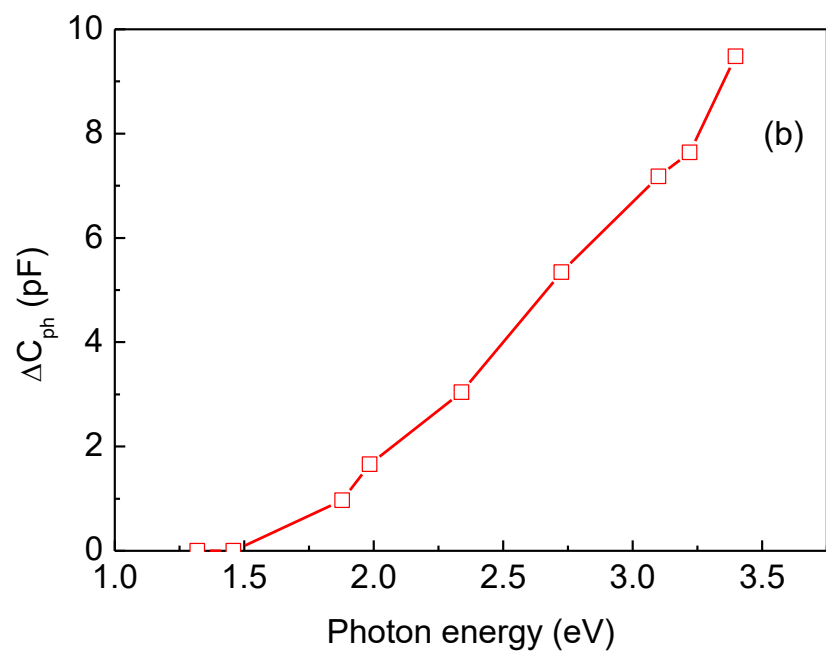
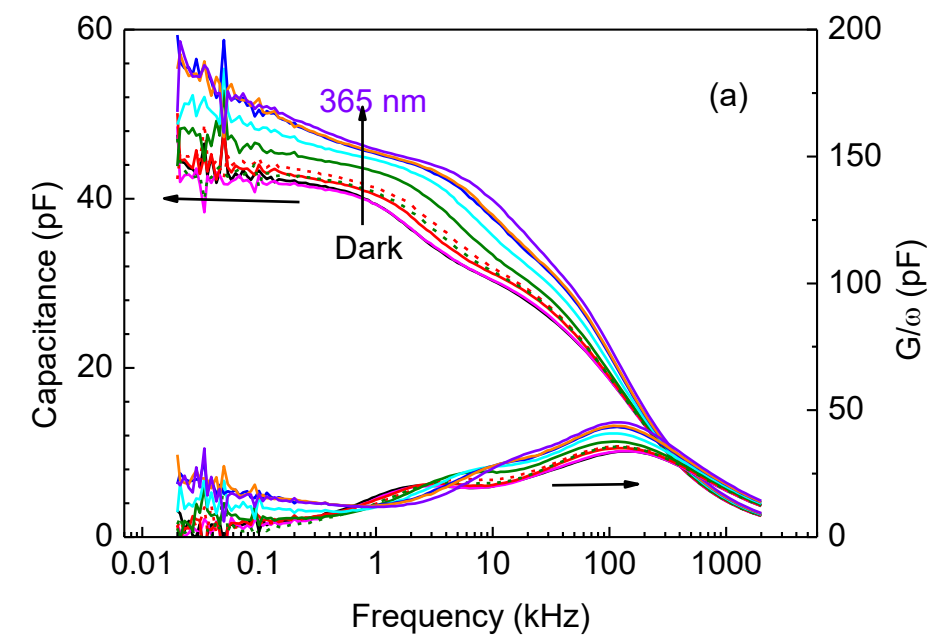
This is the author's peer reviewed, accepted manuscript. However, the online version of record will be different from this version once it has been copyedited and typeset.
PLEASE CITE THIS ARTICLE AS DOI: 10.1063/1.5100359



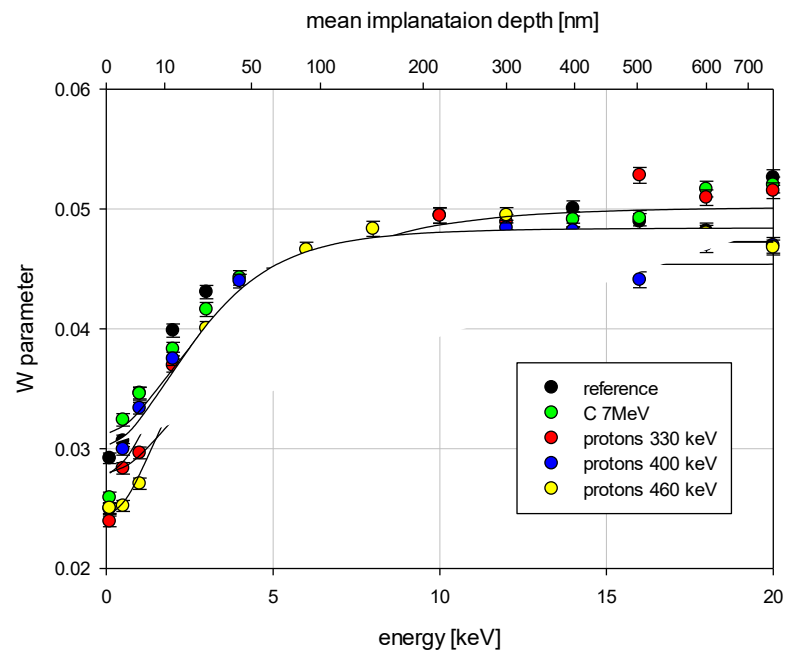
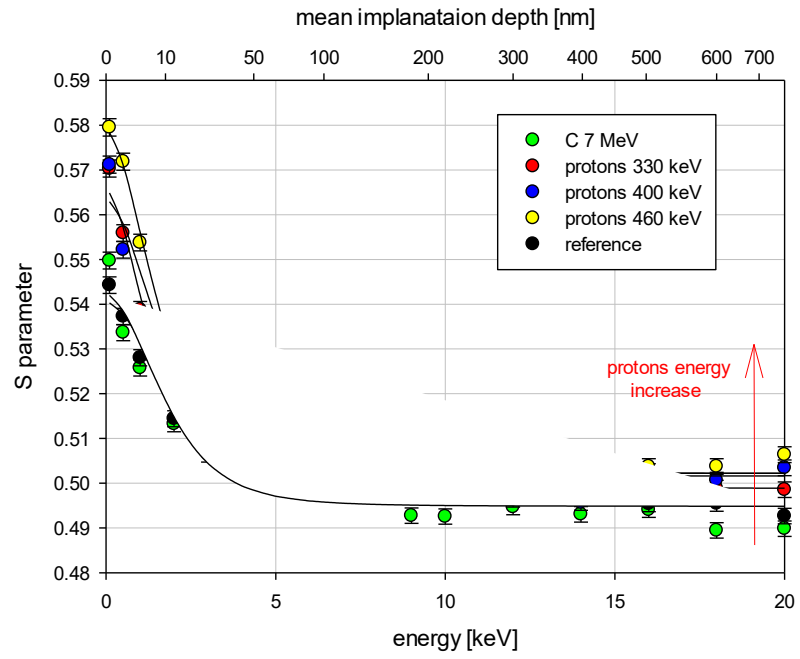
This is the author's peer reviewed, accepted manuscript. However, the online version of record will be different from this version once it has been copyedited and typeset.
PLEASE CITE THIS ARTICLE AS DOI: 10.1063/1.50100359



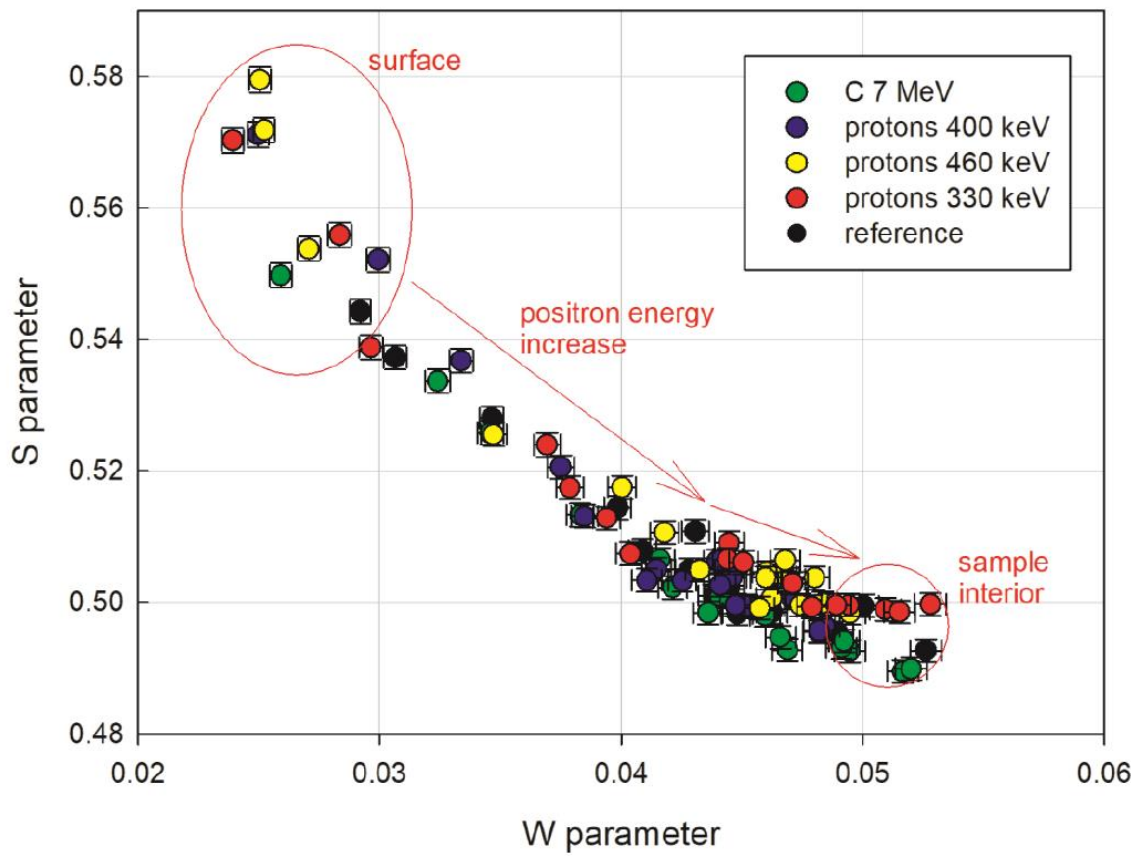
This is the author's peer reviewed, accepted manuscript. However, the online version of record will be different from this version once it has been copyedited and typeset.
PLEASE CITE THIS ARTICLE AS DOI: 10.1063/1.5100359



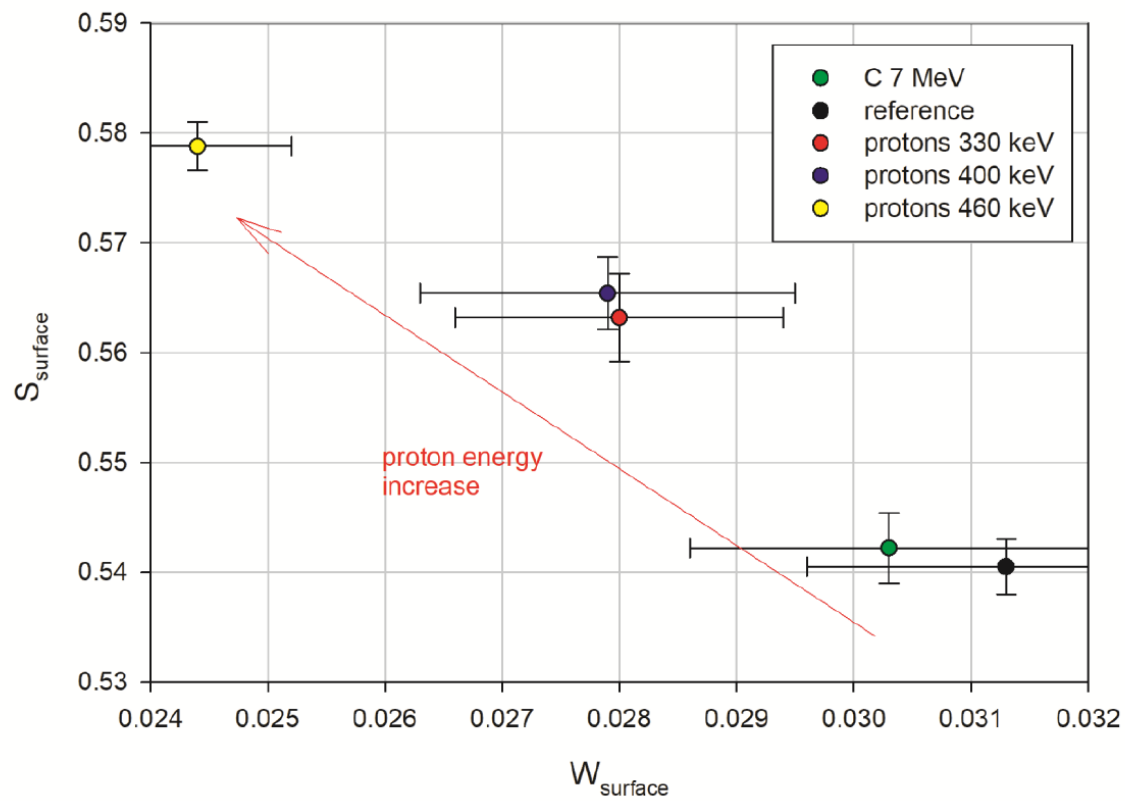
This is the author's peer reviewed, accepted manuscript. However, the online version of record will be different from this version once it has been copyedited and typeset.
 PLEASE CITE THIS ARTICLE AS DOI: 10.1063/5.0100359



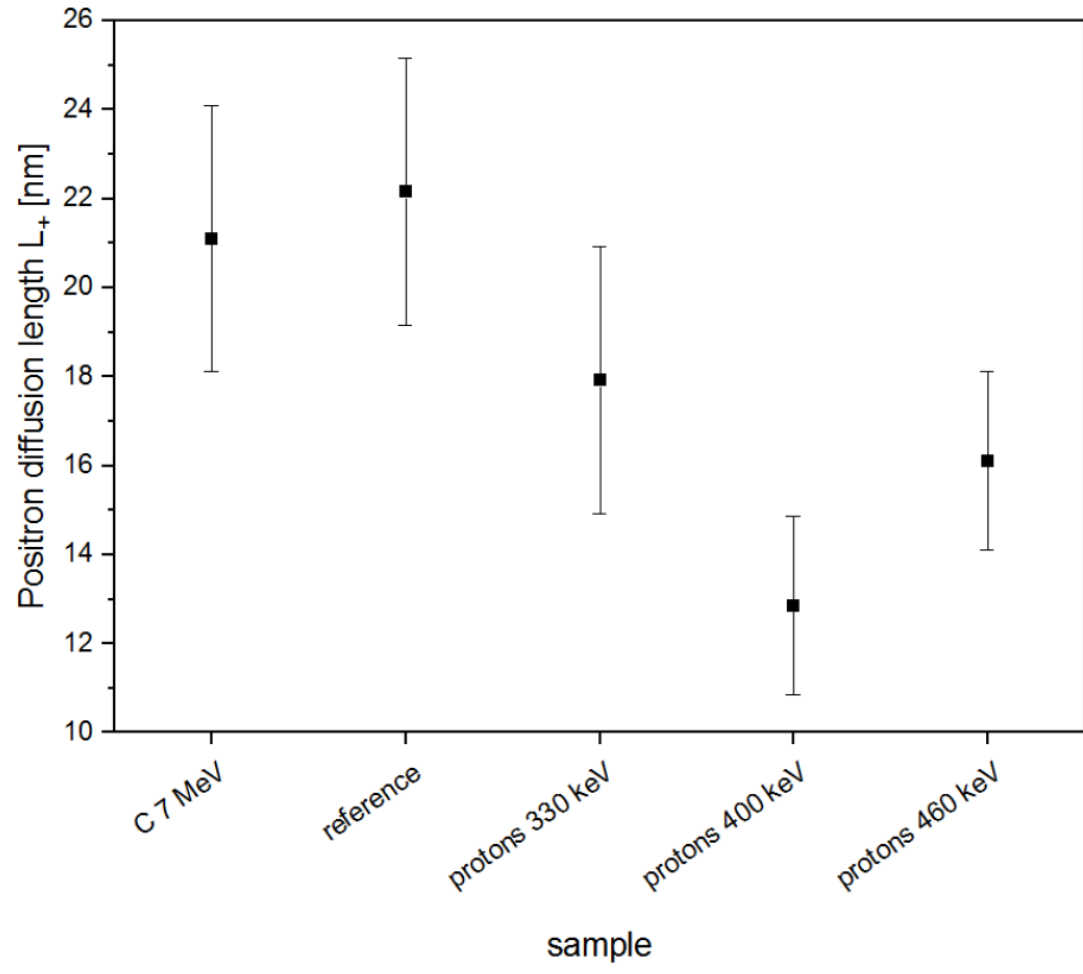
This is the author's peer reviewed, accepted manuscript. However, the online version of record will be different from this version once it has been copyedited and typeset.
 PLEASE CITE THIS ARTICLE AS DOI: 10.1063/1.5100359



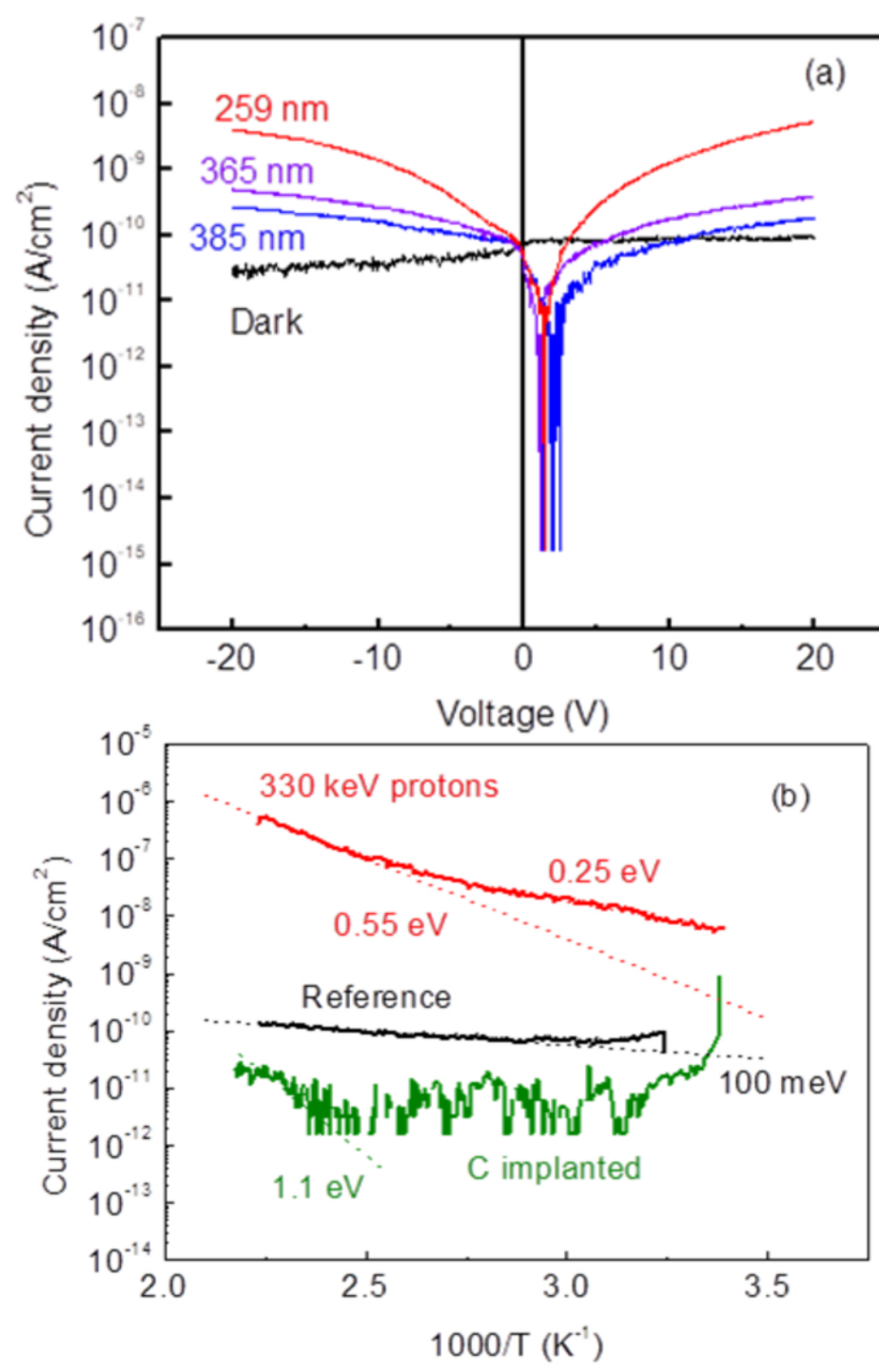
This is the author's peer reviewed, accepted manuscript. However, the online version of record will be different from this version once it has been copyedited and typeset.
PLEASE CITE THIS ARTICLE AS DOI: 10.1063/1.5100359



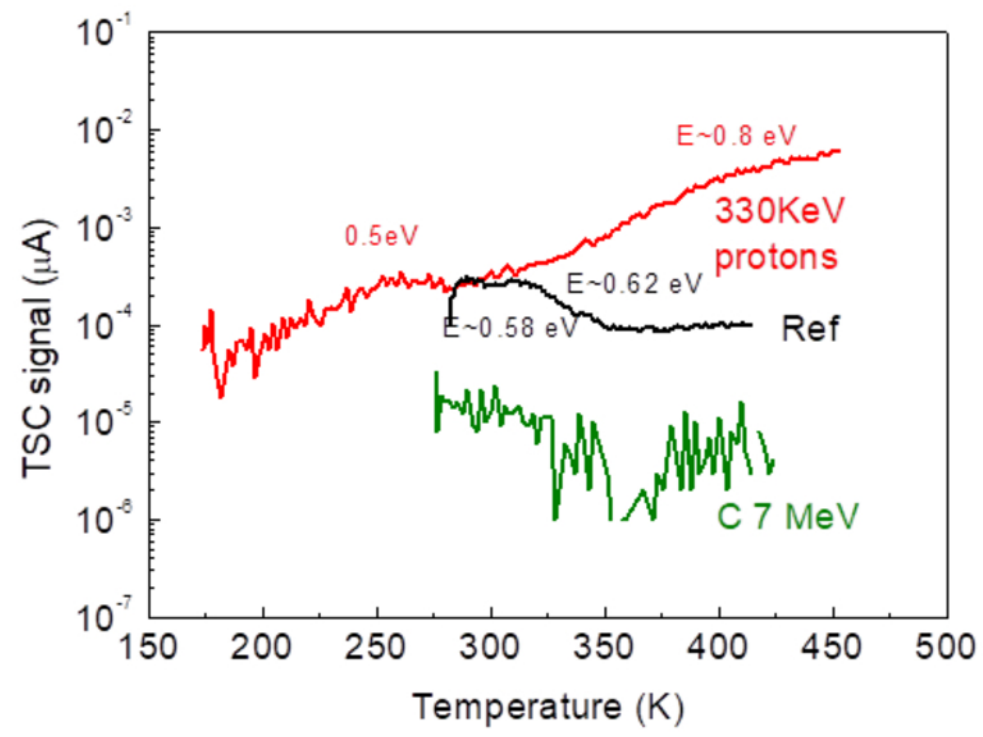
This is the author's peer reviewed, accepted manuscript. However, the online version of record will be different from this version once it has been copyedited and typeset.
PLEASE CITE THIS ARTICLE AS DOI: 10.1063/5.0100359



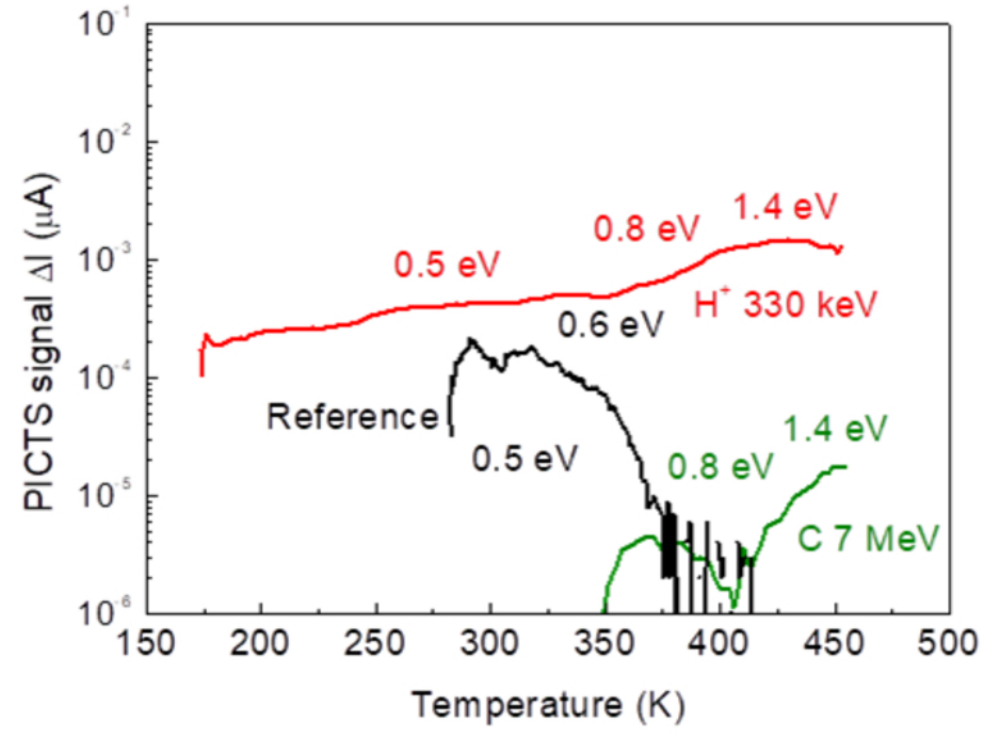
This is the author's peer reviewed, accepted manuscript. However, the online version of record will be different from this version once it has been copyedited and typeset.
PLEASE CITE THIS ARTICLE AS DOI: 10.1063/5.0100359



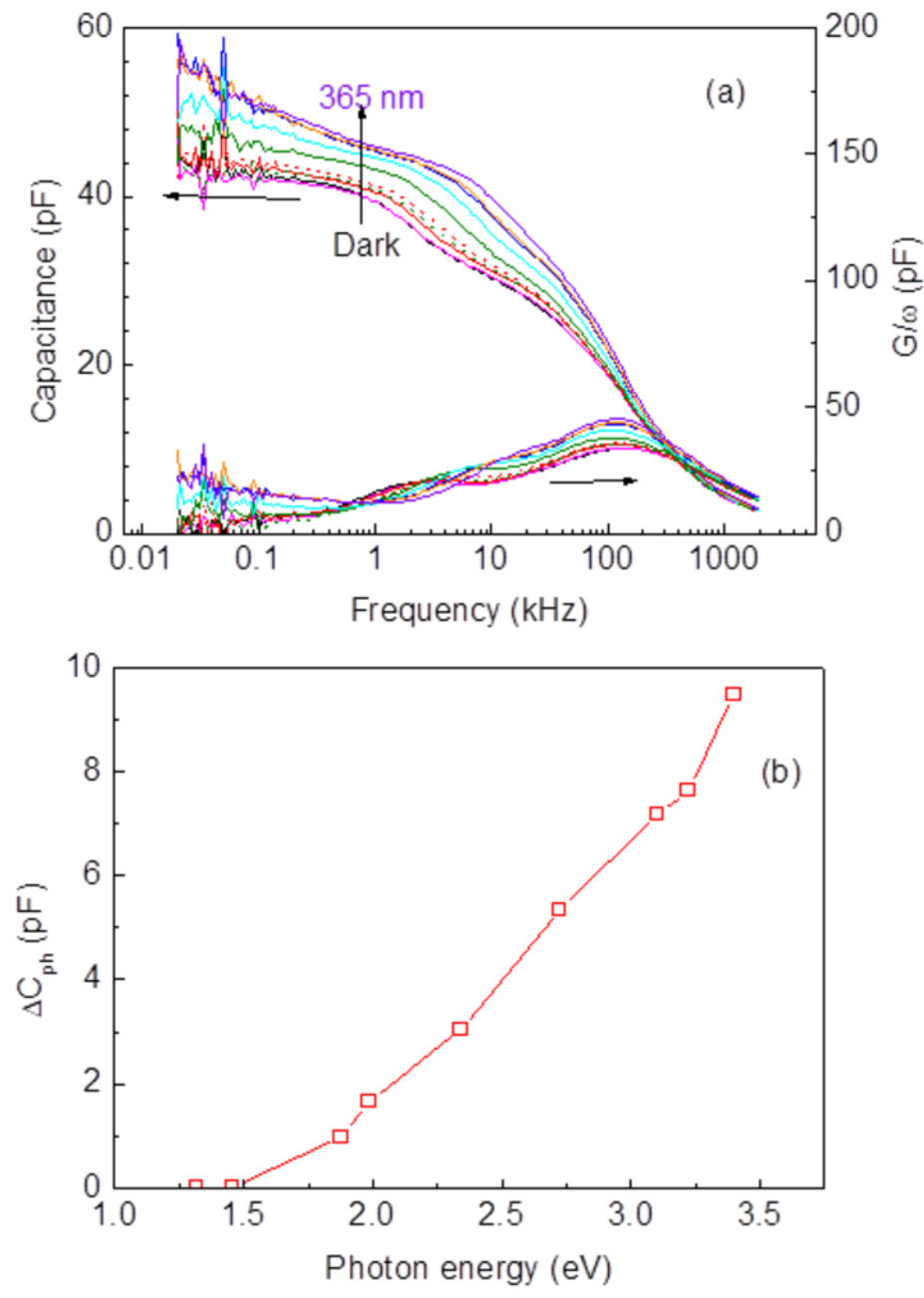
This is the author's peer reviewed, accepted manuscript. However, the online version of record will be different from this version once it has been copyedited and typeset.
PLEASE CITE THIS ARTICLE AS DOI: 10.1063/5.0100359



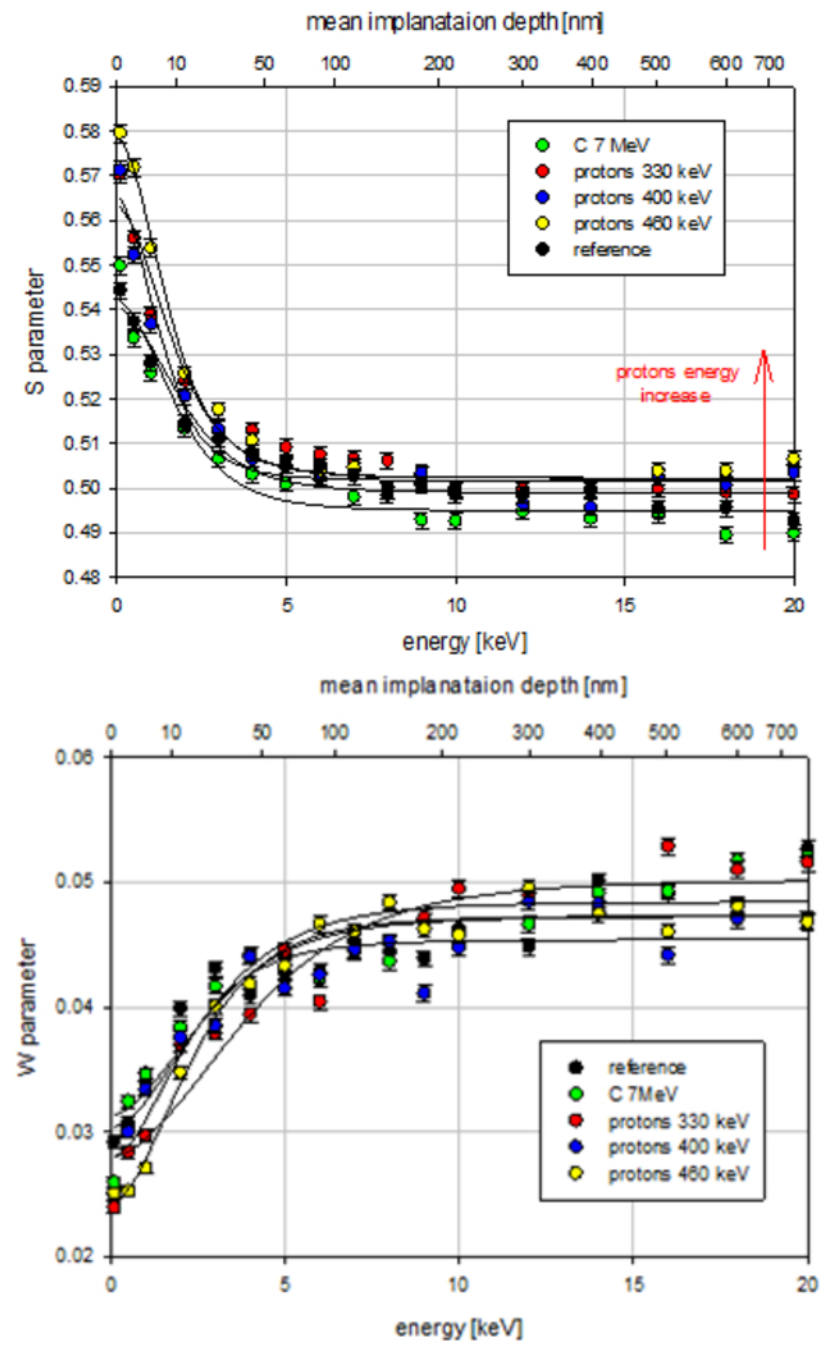
This is the author's peer reviewed, accepted manuscript. However, the online version of record will be different from this version once it has been copyedited and typeset.
PLEASE CITE THIS ARTICLE AS DOI: 10.1063/5.0100359



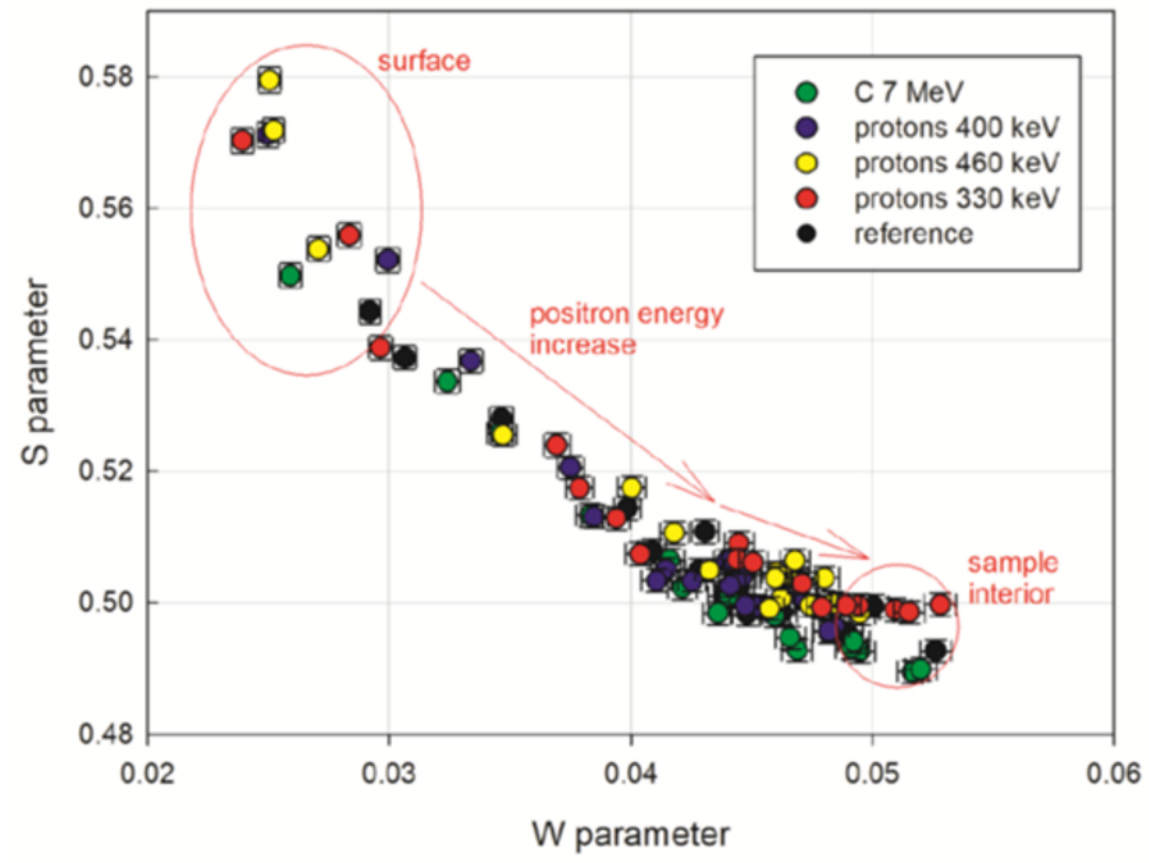
This is the author's peer reviewed, accepted manuscript. However, the online version of record will be different from this version once it has been copyedited and typeset.
PLEASE CITE THIS ARTICLE AS DOI: 10.1063/5.0100359



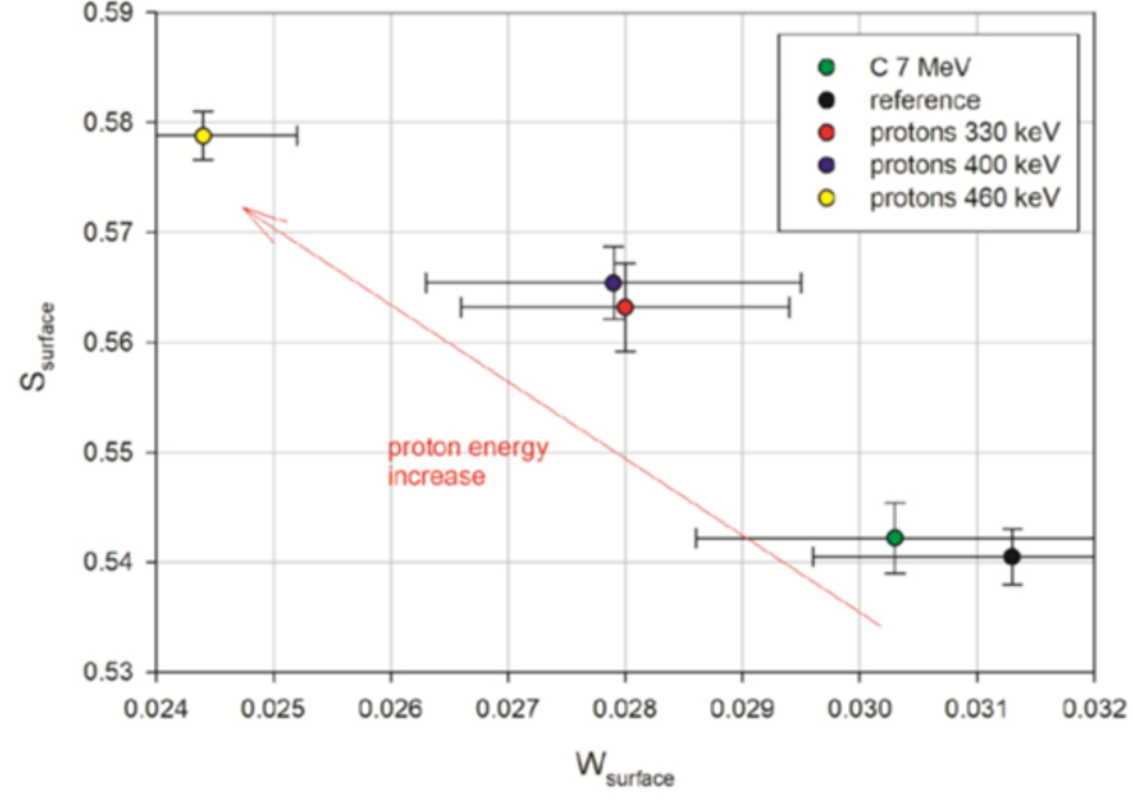
This is the author's peer reviewed, accepted manuscript. However, the online version of record will be different from this version once it has been copyedited and typeset.
PLEASE CITE THIS ARTICLE AS DOI: 10.1063/5.0100359



This is the author's peer reviewed, accepted manuscript. However, the online version of record will be different from this version once it has been copyedited and typeset.
PLEASE CITE THIS ARTICLE AS DOI: 10.1063/5.0100359



This is the author's peer reviewed, accepted manuscript. However, the online version of record will be different from this version once it has been copyedited and typeset.
PLEASE CITE THIS ARTICLE AS DOI: 10.1063/5.0100359



This is the author's peer reviewed, accepted manuscript. However, the online version of record will be different from this version once it has been copyedited and typeset.
PLEASE CITE THIS ARTICLE AS DOI: 10.1063/5.0100359

